

PAPER

Neutrino- ^{13}C cross sections at supernova neutrino energies

To cite this article: T Suzuki *et al* 2019 *J. Phys. G: Nucl. Part. Phys.* **46** 075103

View the [article online](#) for updates and enhancements.



IOP Astronomy ebooks

Part of your publishing universe and your first choice for astronomy, astrophysics, solar physics and planetary science ebooks.

iopscience.org/books/aas

Neutrino- ^{13}C cross sections at supernova neutrino energies

T Suzuki^{1,2}, A B Balantekin^{2,3,7}, T Kajino^{2,4,5} and S Chiba^{2,6}

¹ Department of Physics, College of Humanities and Sciences, Nihon University, Sakurajosui 3-25-40, Setagaya-ku, Tokyo 156-8550, Japan

² National Astronomical Observatory of Japan 2-21-1 Osawa, Mitaka, Tokyo, 181-8588, Japan

³ Department of Physics, University of Wisconsin, Madison, WI 53706, United States of America

⁴ Graduate School of Science, University of Tokyo, 7-3-1 Hongo, Bunkyo-ku, Tokyo, 113-0033, Japan

⁵ School of Physics, Beihang University, Beijing 100083, People's Republic of China

⁶ Laboratory for Advanced Nuclear Energy, Institute of Innovative Research, Tokyo Institute of Technology, N1-9, 2-12-1 Ookayama, Meguro, Tokyo 152-8550, Japan

E-mail: suzuki@phys.chs.nihon-u.ac.jp, baha@physics.wisc.edu and kajino@nao.ac.jp

Received 24 January 2019, revised 10 April 2019

Accepted for publication 24 April 2019

Published 22 May 2019



CrossMark

Abstract

We present neutrino capture cross sections on ^{13}C at supernova neutrino energies, up to 50 MeV. For both charged-current and neutral-current reactions partial cross sections are calculated using the statistical Hauser-Feshbach method. Coherent elastic neutrino scattering cross section for a ^{13}C target is also provided.

Keywords: neutrino cross sections, scintillators, ^{13}C

(Some figures may appear in colour only in the online journal)

1. Introduction

There has been outstanding progress in all aspects of neutrino physics during the past several decades. This progress increasingly necessitates the availability of accurate neutrino-nucleus cross sections. The most reliable calculations of such cross sections at lower energies (defined as reactor, solar and supernova neutrino energies) are based on the nuclear shell model. In parallel to the rapid progress in neutrino physics, new shell model Hamiltonians have been recently developed. These Hamiltonians, including the tensor forces, describe well nuclear

⁷ Author to whom correspondence may be addressed.

spin responses and shell evolution towards the drip lines. Such a new shell model Hamiltonian for p -shell nuclei is the SFO (Suzuki, Fujimoto, Otsuka) Hamiltonian [1].

Many large neutrino experiments such as currently operating Daya Bay [2], RENO [3], Double Chooz [4], BOREXINO [5] experiments, under construction JUNO experiment [6], and the proposed LENA experiment [7] utilize carbon-based liquid scintillators and liquid track detectors. Indeed that is one reason why the neutrino interactions with ^{12}C is experimentally well studied [8]. The natural abundance of ^{13}C is 1.07%, hence in a precision experiment neutrino interactions with ^{13}C are no longer negligible. This cross section has not been directly measured, but may be accessible with a ^{13}C -enriched target. In addition, as we discuss in section 4.2, knowing the exact value of this cross section in the Standard Model would help searches for physics beyond the Standard Model. In the late 1980s a ^{13}C -enriched target was proposed as a possible solar neutrino detector [9], motivating a calculation of this reaction [10] both in the shell model (using Cohen–Kurath (CK) wave functions [11, 12]) and using the effective operator method [13]. Ground-to-ground state transitions and inclusive cross sections were also given [14, 15]. In a previous publication [16] we provided a detailed calculation of the neutrino interactions with ^{13}C using the SFO Hamiltonian at reactor energies. Carbon-based scintillators can be used as supernova detectors [17, 18] and multi-purpose neutrino observatories which use liquid scintillators have been proposed [7]. Sensitivity to all flavors of neutrinos and antineutrinos in a supernova burst is the ultimate goal of a supernova neutrino detector. This goal in turn requires knowing as many as possible cross sections for various potential detectors. The goal of the present paper is to extend our previous calculations of neutrino- ^{13}C cross sections to higher energies, up to about 50 MeV, relevant to supernova observations and experiments at the spallation neutron sources.

2. Calculations with the SFO Hamiltonian

Starting from the CK [11] and the Millener–Kurath (MK) [12] Hamiltonians, a new shell model Hamiltonian for the p - sd shell has been constructed. The CK Hamiltonians are phenomenological effective interactions for the p -shell obtained by fitting experimental low-lying energy levels. In one version, (8–16)2BE, single-particle energies for $p_{1/2}$ and $p_{3/2}$ orbits and two-body matrix elements are determined by using 35 energy data for nuclei with mass numbers $A = 8$ –16. The MK Hamiltonian is an effective particle-hole interaction for p - sd cross shell obtained by fitting to energy levels of non-normal parity states of nuclei with $A = 11$ –16. The strength parameters of central, tensor and two-body spin–orbit potentials are determined. The new Hamiltonian for the p - sd shell, SFO [1], consists of p shell, sd shell and p - sd shell parts, where $\langle p, sd|V|p, sd \rangle$ part is taken from the MK Hamiltonian while $\langle p^2|V|(sd)^2 \rangle$ and sd shell parts are from Kuo’s G -matrix calculation [19]. The p -shell part is modified from (8–16)2BME by enhancing the magnitude of the monopole terms of the matrix elements for the $p_{1/2}$ – $p_{3/2}$ orbits with zero isospin as well as the single-particle energy gap between the $p_{1/2}$ and $p_{3/2}$ orbits. The monopole term is changed by -2.14 MeV and the gap is enhanced from 0.14 to 3.92 MeV.

Using a configuration space including up to $2\hbar\omega$ excitations and a small (5%) quenching of the axial-vector coupling constant and spin g factor, this Hamiltonian considerably improves the magnetic properties of the p -shell nuclei as compared with the earlier treatments using CK interactions. For example, the Gamow–Teller strength in ^{12}C is well described by the SFO Hamiltonian, resulting in a good agreement with the experimental measurements [20]. The enhancement of the magnitude of the monopole terms in the spin-isospin flip channel leads to more admixtures of $p_{1/2}$ and $p_{3/2}$ shell components in the wave functions and

reduction of the $B(GT)$ strength. The enhancement of the single-particle energy gap, on the other hand, leads to less admixtures of $p_{1/2}$ and $p_{3/2}$ shell components and enhancement of the $B(GT)$ value. Spin and magnetic properties of nuclei are sensitive to the balance between the monopole terms and the single-particle energy gap. Their proper choice is important for the description of the spin degree's of freedom in nuclei. The SFO Hamiltonian contains the proper tensor components consistent with the sign rules for the monopole-tensor terms [21], that is, attractive for j_j-j_k orbits ($j_j = \ell + 1/2$, $j_k = \ell - 1/2$) but repulsive for j_j-j_j or j_k-j_k orbits. The spin-isospin dependent part of the SFO interaction is strong enough to be consistent with this sign rule, while the CK interaction contains the tensor components with opposite signs to the proper ones due to its weak monopole terms in the spin-isospin flip channel [20]. The description of spin and magnetic properties of p -shell nuclei is thus improved for the SFO Hamiltonian compared with the CK Hamiltonians. The SFO interaction is found to reproduce well the exclusive cross section $^{12}\text{C}(\nu_e, e^-)^{12}\text{N}(1_{\text{g.s.}}^+)$ as well as charged- and neutral-current inclusive reaction cross sections on ^{12}C induced by pion DAR (decay-at-rest) neutrinos within error bars [20, 22]. In particular in figure 4 of [22], the exclusive cross section measured (figure 14 of [8]), which is not folded over the DAR spectrum, is shown to be reproduced by SFO quite well. Another successful example of SFO interaction is the Gamow–Teller strength in ^{14}C [1]. The $B(GT)$ strength is found to be almost vanished for the SFO interaction, where the proper inclusion of the tensor components in the interaction is essential. Note that the calculations with the SFO Hamiltonian are carried out in the p - sd shell including up to $2\hbar\omega$ excitations with $g_A^{\text{eff}}/g_A = 0.95$, whereas those for the comparison CK Hamiltonian are obtained within the p -shell with a larger quenching factor, $g_A^{\text{eff}}/g_A = 0.69$ [10], which is adjusted to reproduce the experimental $B(GT)$ values of $^{13}\text{N}(\beta^+)^{13}\text{C}$, $^{15}\text{O}(\beta^+)^{15}\text{N}$ and $^{11}\text{C}(\beta^+)^{11}\text{B}$. For the charged-current neutrino scattering on ^{13}C the SFO Hamiltonian predicts an enhancement of the Gamow–Teller strength for the transition to the 3.50 MeV $3/2^-$ state in ^{13}N as compared with the prediction of the CK Hamiltonian [16].

In our calculations neutrino-nucleus reaction cross sections are evaluated using the multipole expansion of the weak hadronic currents as described in [23]. To calculate partial cross sections for the photon and particle emission channels statistical Hauser-Feshbach method is used. Branching ratios from each excited level are evaluated by taking into account single- and multiparticle decay channels involving neutron, proton, deuteron, α , ^3He , ^3H and γ . All the levels obtained in the present shell model calculations are adopted as levels in the decaying and daughter nuclei with specific isospin assignments. The particle transmission coefficients are calculated by the optical model [24, 25]. The γ transmission coefficients are calculated with the Brink formula. The E1 (electric dipole) and M1 (magnetic dipole) parameters are taken from RIPL-2 database [26]. The γ cascade in the initial excited nuclei and subsequent decays are fully considered.

3. Charged-current cross sections

We present the total charged-current cross sections for $\nu_e-^{13}\text{C}$ scattering in table 1. The cross sections given in this table include all possible channels. The most dominant contribution to the total cross section comes from the proton knock-out reaction

$$\nu_e + ^{13}\text{C} \rightarrow ^{12}\text{C} + e^- + p. \quad (3.1)$$

This cross section is given in table 2. This partial cross section can be observed if the scintillator is capable of pulse-shape discrimination. The second dominant contribution comes

Table 1. Total cross section for the charged current reaction $^{13}\text{C}(\nu_e, e^-X)$ with all channels included.

$E_\nu(\text{MeV})$	$\sigma \text{ (cm}^2\text{)}$	$E_\nu(\text{MeV})$	$\sigma \text{ (cm}^2\text{)}$	$E_\nu(\text{MeV})$	$\sigma \text{ (cm}^2\text{)}$	$E_\nu(\text{MeV})$	$\sigma \text{ (cm}^2\text{)}$
3	2.21×10^{-44}	16	1.32×10^{-41}	29	6.87×10^{-41}	42	1.80×10^{-40}
4	9.39×10^{-44}	17	1.59×10^{-41}	30	7.50×10^{-41}	43	1.92×10^{-40}
5	2.23×10^{-43}	18	1.86×10^{-41}	31	8.18×10^{-41}	44	2.03×10^{-40}
6	4.39×10^{-43}	19	2.17×10^{-41}	32	8.89×10^{-41}	45	2.15×10^{-40}
7	8.38×10^{-43}	20	2.51×10^{-41}	33	9.62×10^{-41}	46	2.28×10^{-40}
8	1.41×10^{-42}	21	2.88×10^{-41}	34	1.04×10^{-40}	47	2.41×10^{-40}
9	2.16×10^{-42}	22	3.27×10^{-41}	35	1.12×10^{-40}	48	2.56×10^{-40}
10	3.10×10^{-42}	23	3.70×10^{-41}	36	1.21×10^{-40}	49	2.70×10^{-40}
11	4.20×10^{-42}	24	4.15×10^{-41}	37	1.29×10^{-40}	50	2.84×10^{-40}
12	5.52×10^{-42}	25	4.62×10^{-41}	38	1.38×10^{-40}	51	2.99×10^{-40}
13	7.09×10^{-42}	26	5.14×10^{-41}	39	1.48×10^{-40}	52	3.15×10^{-40}
14	8.90×10^{-42}	27	5.69×10^{-41}	40	1.59×10^{-40}	53	3.31×10^{-40}
15	1.09×10^{-41}	28	6.26×10^{-41}	41	1.70×10^{-40}	54	3.47×10^{-40}

Table 2. Cross section for the charged current reaction $^{13}\text{C} (\nu_e, e^- p) ^{12}\text{C}$.

$E_\nu(\text{MeV})$	$\sigma \text{ (cm}^2\text{)}$	$E_\nu(\text{MeV})$	$\sigma \text{ (cm}^2\text{)}$	$E_\nu(\text{MeV})$	$\sigma \text{ (cm}^2\text{)}$	$E_\nu(\text{MeV})$	$\sigma \text{ (cm}^2\text{)}$
5	1.85×10^{-46}	17	9.76×10^{-42}	29	4.85×10^{-41}	41	1.23×10^{-40}
6	3.05×10^{-44}	18	1.18×10^{-41}	30	5.32×10^{-41}	42	1.31×10^{-40}
7	1.86×10^{-43}	19	1.40×10^{-41}	31	5.82×10^{-41}	43	1.39×10^{-40}
8	4.62×10^{-43}	20	1.65×10^{-41}	32	6.35×10^{-41}	44	1.47×10^{-40}
9	8.60×10^{-43}	21	1.88×10^{-41}	33	6.90×10^{-41}	45	1.57×10^{-40}
10	1.14×10^{-42}	22	2.19×10^{-41}	34	7.47×10^{-41}	46	1.66×10^{-40}
11	2.03×10^{-42}	23	2.50×10^{-41}	35	8.09×10^{-41}	47	1.76×10^{-40}
12	2.84×10^{-42}	24	2.84×10^{-41}	36	8.71×10^{-41}	48	1.83×10^{-40}
13	3.84×10^{-42}	25	3.19×10^{-41}	37	9.37×10^{-41}	49	1.95×10^{-40}
14	5.02×10^{-42}	26	3.56×10^{-41}	38	1.01×10^{-40}	50	2.05×10^{-40}
15	6.40×10^{-42}	27	3.99×10^{-41}	39	1.07×10^{-40}	51	2.16×10^{-40}
16	7.98×10^{-42}	28	4.39×10^{-41}	40	1.15×10^{-40}	52	2.26×10^{-40}

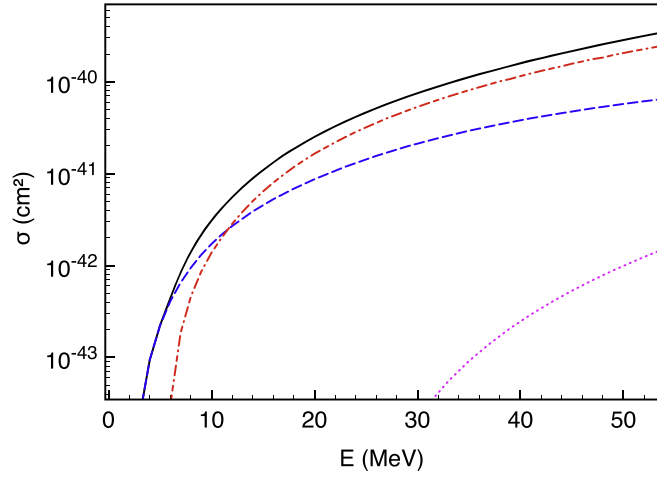
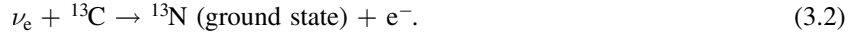
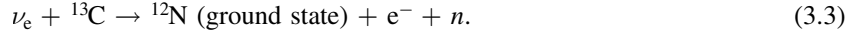


Figure 1. Total charged current cross section for the $\nu_e + {}^{13}\text{C}$ reaction (solid line) as a function of the incoming neutrino energy. Also shown are the two major contributions to the total cross section: the proton emission cross section of equation (3.1) (dotted-dashed line) and transition to the ground state of ${}^{13}\text{N}$ (equation (3.2), dashed line), and the neutron emission cross section (equation (3.3), dotted line). To avoid cluttering of the figure several other contributions the same order as the neutron emission cross section are not shown.

from the reaction



Of significant interest is the neutron emission cross section



These neutrons thermalize and capture abundant protons typically present in the scintillators, giving the characteristic signature of 2.2 MeV photons. However the cross section for the reaction in equation (3.3) is much smaller than the two dominant contributions mentioned previously as depicted in figure 1. (Note that to avoid cluttering several other contributions which are the same order as the neutron emission cross section are not shown in this figure. These contributions come from emissions of photons, proton pairs, proton-neutron pairs, one proton and one alpha pairs or one proton along with a pair of alpha particles, but they are too small to be directly detectable.)

The charged-current electron antineutrino capture cross section on ${}^{13}\text{C}$ has a relatively high energy threshold (~ 16 MeV). In addition it is much smaller than the charged-current electron neutrino cross section on ${}^{13}\text{C}$. We compare those two cross section is figure 2. ${}^{12}\text{C}$ also has a relatively high energy threshold for both electron neutrinos and electron antineutrinos. Hence a scintillator containing ${}^{12}\text{C}$, ${}^{13}\text{C}$ and protons is sensitive to electron neutrinos only via their capture on ${}^{13}\text{C}$ and can be used to search for new physics producing electron neutrinos in reactor flux. This is why such scintillators were also proposed as solar neutrino detectors [10, 27]. It should also be mentioned that neutrinos coming from spallation neutron sources contain electron neutrinos in addition to muon neutrinos and antineutrinos; however electron antineutrinos are absent from their spectra [28].

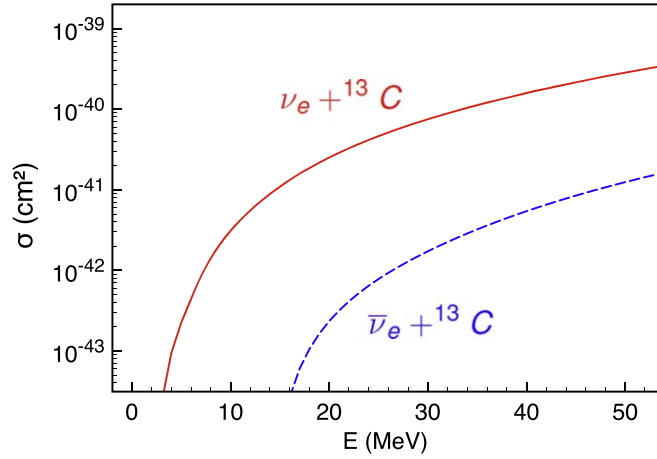


Figure 2. Total charged current cross sections for the $\nu_e + {}^{13}\text{C}$ reaction (solid line) and $\bar{\nu}_e + {}^{13}\text{C}$ reaction (dashed line) as a function of the incoming neutrino energy.

4. Neutral-current cross sections

4.1. Neutrino coherent scattering

Neutrino-nucleus coherent elastic scattering cross section is given by [29–31]

$$\frac{d\sigma}{dT}(E, T) = \frac{G_F^2}{8\pi} M \left[2 - \frac{2T}{T_{\max}} + \left(\frac{T}{E} \right)^2 \right] Q_W^2 [F(Q^2)]^2, \quad (4.1)$$

where T is the recoil energy of the nucleus, E is the energy of the incoming neutrino, M is the mass of the target nucleus, Q^2 is the momentum transfer, T_{\max} is the maximum nuclear recoil energy

$$T_{\max} = \frac{2E^2}{2E + M}, \quad (4.2)$$

and

$$Q_W = N - (1 - 4 \sin^2 \theta_W)Z$$

is the weak charge of the nucleus. The form factor

$$F(Q^2) = \frac{1}{Q_W} \int dr \, r^2 \frac{\sin(Qr)}{Qr} [\rho_n(r) - (1 - 4 \sin^2 \theta_W) \rho_p(r)] \quad (4.3)$$

corrects for contributions to scattering that are not completely coherent as E gets large. In this expression ρ_n and ρ_p are the neutron and proton density distributions in the nucleus, respectively. In writing equation (4.3) nuclei are assumed to be at least nearly spherically symmetric. This reaction was experimentally observed for the first time only recently using a CsI scintillator [32].

The total elastic scattering cross section is given by the expression

$$\sigma(E) = \int_0^{T_{\max}} dT \frac{d\sigma}{dT}(E, T). \quad (4.4)$$

Table 3. Total cross section for neutrino-¹³C elastic scattering.

$E_\nu(\text{MeV})$	$\sigma \text{ (cm}^2\text{)}$	$E_\nu(\text{MeV})$	$\sigma \text{ (cm}^2\text{)}$	$E_\nu(\text{MeV})$	$\sigma \text{ (cm}^2\text{)}$	$E_\nu(\text{MeV})$	$\sigma \text{ (cm}^2\text{)}$
1	1.47×10^{-43}	15	3.96×10^{-41}	29	1.41×10^{-40}	43	2.89×10^{-40}
2	6.77×10^{-43}	16	4.49×10^{-41}	30	1.51×10^{-40}	44	3.01×10^{-40}
3	1.58×10^{-42}	17	5.06×10^{-41}	31	1.60×10^{-40}	45	3.13×10^{-40}
4	2.83×10^{-42}	18	5.66×10^{-41}	32	1.70×10^{-40}	46	3.25×10^{-40}
5	4.45×10^{-42}	19	6.28×10^{-41}	33	1.80×10^{-40}	47	3.37×10^{-40}
6	6.39×10^{-42}	20	6.94×10^{-41}	34	1.90×10^{-40}	48	3.49×10^{-40}
7	8.69×10^{-42}	21	7.63×10^{-41}	35	2.00×10^{-40}	49	3.61×10^{-40}
8	1.14×10^{-41}	22	8.35×10^{-41}	36	2.11×10^{-40}	50	3.74×10^{-40}
9	1.44×10^{-41}	23	9.09×10^{-41}	37	2.21×10^{-40}	51	3.86×10^{-40}
10	1.77×10^{-41}	24	9.87×10^{-41}	38	2.32×10^{-40}	52	3.98×10^{-40}
11	2.14×10^{-41}	25	1.07×10^{-40}	39	2.43×10^{-40}	53	4.11×10^{-40}
12	2.54×10^{-41}	26	1.15×10^{-40}	40	2.55×10^{-40}	54	4.24×10^{-40}
13	2.98×10^{-41}	27	1.24×10^{-40}	41	2.66×10^{-40}	55	4.49×10^{-40}
14	3.45×10^{-41}	28	1.32×10^{-40}	42	2.77×10^{-40}	56	4.62×10^{-40}

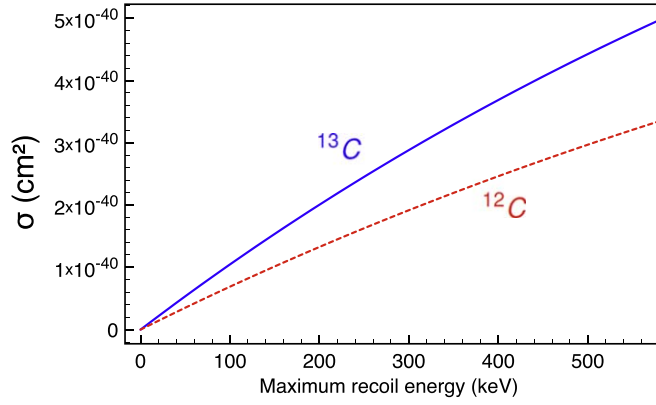


Figure 3. Neutrino elastic scattering cross sections on ^{13}C (solid line) and ^{12}C (dashed line) as a function of the *maximum* nuclear recoil energy. The ^{12}C cross section is taken from [33].

We present the total elastic scattering cross section for ^{13}C in table 3. Note that the nuclear recoil energies are very small. However, due to the extra neutron, neutrino elastic scattering from ^{13}C is significantly more than the similar reaction of ^{12}C . To illustrate this we compare the elastic scattering cross sections on ^{13}C and ^{12}C in figure 3 as a function of the maximum nuclear recoil energy. In this figure the coherent scattering cross section for ^{12}C is taken from [33]. As this figure illustrates even a single extra neutron appreciably increases the coherent scattering cross section.

In [34] an expansion of the form factor in equation (4.3) was given in powers of the momentum transfer, Q^2 . Since the proton contribution to the form factor is exceedingly small, neutrino coherent scattering primarily probes the neutron distribution. In the leading order the momentum transfer is given by

$$Q^2 \sim 2MT. \quad (4.5)$$

For lighter nuclei an expansion of the form factor can be written as

$$F(Q^2) = 1 + \eta_2 Q^2 + \eta_4 Q^4 + \dots, \quad (4.6)$$

where the coefficients η_i carry information about the neutron distribution. It can be shown that keeping terms up to and including Q^4 in the expansion of equation (4.6) contributes terms up to and including E^6 in the total cross section. This feature can be observed by writing the total cross section as an expansion:

$$\sigma(E) = \frac{G_F^2}{8\pi} Q_W^2 \left[x + \frac{4}{3} \eta_2 x^2 + \frac{1}{3} \left(2(\eta_2^2 + 2\eta_4) x^3 + \frac{x^3}{(ME)^2} \right) + \dots \right], \quad (4.7)$$

where $x = MT_{\text{max}}$. The following expansion of this expression may be more useful in applications:

$$\begin{aligned} \sigma(E) = \frac{G_F^2}{4\pi} Q_W^2 E^2 & \left[\left(1 + \frac{8}{3} \eta_2 E^2 + \frac{8}{3} (\eta_2^2 + 2\eta_4) E^4 + \dots \right) \right. \\ & \left. - \frac{2}{M} \left(E + \frac{16}{3} \eta_2 E^3 + \frac{24}{3} (\eta_2^2 + 2\eta_4) E^5 + \dots \right) + \dots \right]. \end{aligned} \quad (4.8)$$

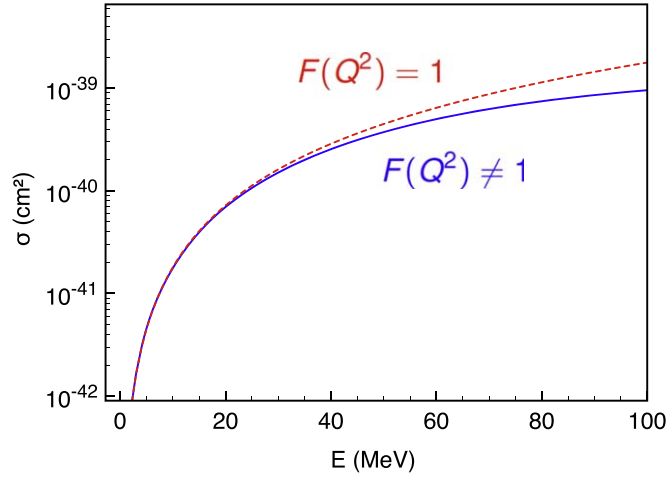


Figure 4. Total neutrino elastic scattering cross sections on ^{13}C (solid line). The prediction of equation (4.1) with $F(Q^2) = 1$ is also shown (dashed line).

For ^{13}C with only seven neutrons the contribution of even η_4 term is exceedingly small. In figure 4 we give a comparison of the total neutrino elastic scattering cross sections on ^{13}C and the prediction of equation (4.1) with $F(Q^2) = 1$. Clearly nuclear structure effects decrease the cross section from the value given in the limit where deviations from $F(Q^2) = 1$ are ignored. It is important to include such effects when one is exploring the decrease of the elastic scattering cross section due to other physical effects such as possible production of sterile neutrinos. One should also mention that, since oscillations experiments established the non-zero values of the neutrino masses, dipole moments of neutrinos do not vanish, very small in the Standard Model, but may receive contributions from physics beyond the Standard Model. Such magnetic moments would provide an electromagnetic contribution to the coherent scattering, but that contribution is expected to be exceedingly small.

4.2. Neutron knock-out

One interesting aspect of the neutral-current scattering of neutrinos and antineutrinos on ^{13}C is the possibility of one neutron emission in the final state. These neutrons are detectable via the 2.2 MeV photons and can provide a useful signal. In these cross sections there are contributions from interference between vector and axial-vector currents, which have different signs between left-handed neutrinos and right-handed antineutrinos. This feature leads to a small difference between (ν, ν') and $(\bar{\nu}, \bar{\nu}')$ cross sections. The total neutron emission cross sections are given in table 4. These cross sections have several components which can help analysis of data from supernova and neutron-spallation sources. These are compared in figure 5. In this figure the small difference between neutrino and antineutrino cross sections described previously, comparable to the width of lines drawn, is ignored. The solid line refers to the total neutral-current one-neutron emission cross section. The dashed line refers to the cross section for transition to the 0^+ ground state in ^{12}C :

$$\nu + ^{13}\text{C} \rightarrow \nu + n + ^{12}\text{C}(\text{g.s.}), \quad (4.9)$$

and the dotted line refers to the cross section for transition to the 2^+ state in ^{12}C at 4.44 MeV followed by decay into the ^{12}C ground state:

Table 4. Total cross sections for the neutral-current $\nu + {}^{13}\text{C}$ and $\bar{\nu} + {}^{13}\text{C}$ reactions with one neutron in the final state.

E (MeV)	$\sigma(\nu + {}^{13}\text{C})$ (cm ²)	$\sigma(\bar{\nu} + {}^{13}\text{C})$ (cm ²)	E (MeV)	$\sigma(\nu + {}^{13}\text{C})$ (cm ²)	$\sigma(\bar{\nu} + {}^{13}\text{C})$ (cm ²)
6.00	$0.161\,144 \times 10^{-55}$	$0.616\,611 \times 10^{-55}$	34.00	$0.548\,597 \times 10^{-41}$	$0.464\,032 \times 10^{-41}$
7.00	$0.498\,686 \times 10^{-48}$	$0.808\,538 \times 10^{-49}$	35.00	$0.601\,253 \times 10^{-41}$	$0.505\,865 \times 10^{-41}$
8.00	$0.170\,467 \times 10^{-46}$	$0.418\,146 \times 10^{-47}$	36.00	$0.656\,985 \times 10^{-41}$	$0.549\,798 \times 10^{-41}$
9.00	$0.144\,971 \times 10^{-45}$	$0.863\,204 \times 10^{-46}$	37.00	$0.715\,877 \times 10^{-41}$	$0.595\,865 \times 10^{-41}$
10.00	$0.492\,129 \times 10^{-44}$	$0.461\,908 \times 10^{-44}$	38.00	$0.778\,015 \times 10^{-41}$	$0.644\,095 \times 10^{-41}$
11.00	$0.208\,600 \times 10^{-43}$	$0.197\,935 \times 10^{-43}$	39.00	$0.843\,485 \times 10^{-41}$	$0.694\,513 \times 10^{-41}$
12.00	$0.506\,791 \times 10^{-43}$	$0.480\,249 \times 10^{-43}$	40.00	$0.912\,365 \times 10^{-41}$	$0.747\,139 \times 10^{-41}$
13.00	$0.947\,193 \times 10^{-43}$	$0.893\,967 \times 10^{-43}$	41.00	$0.984\,743 \times 10^{-41}$	$0.802\,002 \times 10^{-41}$
14.00	$0.154\,234 \times 10^{-42}$	$0.144\,903 \times 10^{-42}$	42.00	$0.106\,069 \times 10^{-40}$	$0.859\,116 \times 10^{-41}$
15.00	$0.229\,880 \times 10^{-42}$	$0.214\,934 \times 10^{-42}$	43.00	$0.114\,029 \times 10^{-40}$	$0.918\,500 \times 10^{-41}$
16.00	$0.322\,241 \times 10^{-42}$	$0.299\,761 \times 10^{-42}$	44.00	$0.122\,361 \times 10^{-40}$	$0.980\,158 \times 10^{-41}$
17.00	$0.431\,917 \times 10^{-42}$	$0.399\,709 \times 10^{-42}$	45.00	$0.131\,073 \times 10^{-40}$	$0.104\,410 \times 10^{-40}$
18.00	$0.559\,371 \times 10^{-42}$	$0.514\,967 \times 10^{-42}$	46.00	$0.140\,169 \times 10^{-40}$	$0.111\,034 \times 10^{-40}$
19.00	$0.705\,006 \times 10^{-42}$	$0.645\,647 \times 10^{-42}$	47.00	$0.149\,658 \times 10^{-40}$	$0.117\,888 \times 10^{-40}$
20.00	$0.869\,271 \times 10^{-42}$	$0.791\,903 \times 10^{-42}$	48.00	$0.159\,545 \times 10^{-40}$	$0.124\,970 \times 10^{-40}$
21.00	$0.105\,267 \times 10^{-41}$	$0.953\,917 \times 10^{-42}$	49.00	$0.169\,835 \times 10^{-40}$	$0.132\,282 \times 10^{-40}$
22.00	$0.125\,572 \times 10^{-41}$	$0.113\,190 \times 10^{-41}$	50.00	$0.180\,532 \times 10^{-40}$	$0.139\,820 \times 10^{-40}$
23.00	$0.147\,902 \times 10^{-41}$	$0.132\,610 \times 10^{-41}$	51.00	$0.191\,641 \times 10^{-40}$	$0.147\,584 \times 10^{-40}$
24.00	$0.172\,324 \times 10^{-41}$	$0.153\,684 \times 10^{-41}$	52.00	$0.203\,165 \times 10^{-40}$	$0.155\,572 \times 10^{-40}$
25.00	$0.198\,912 \times 10^{-41}$	$0.176\,455 \times 10^{-41}$	53.00	$0.215\,107 \times 10^{-40}$	$0.163\,783 \times 10^{-40}$
26.00	$0.227\,737 \times 10^{-41}$	$0.200\,959 \times 10^{-41}$	54.00	$0.227\,470 \times 10^{-40}$	$0.172\,212 \times 10^{-40}$
27.00	$0.258\,877 \times 10^{-41}$	$0.227\,231 \times 10^{-41}$	55.00	$0.240\,256 \times 10^{-40}$	$0.180\,857 \times 10^{-40}$
28.00	$0.292\,406 \times 10^{-41}$	$0.255\,312 \times 10^{-41}$	56.00	$0.253\,465 \times 10^{-40}$	$0.189\,715 \times 10^{-40}$
29.00	$0.328\,421 \times 10^{-41}$	$0.285\,245 \times 10^{-41}$	57.00	$0.267\,098 \times 10^{-40}$	$0.198\,781 \times 10^{-40}$
30.00	$0.366\,993 \times 10^{-41}$	$0.317\,070 \times 10^{-41}$	58.00	$0.281\,156 \times 10^{-40}$	$0.208\,052 \times 10^{-40}$
31.00	$0.408\,214 \times 10^{-41}$	$0.350\,828 \times 10^{-41}$	59.00	$0.295\,636 \times 10^{-40}$	$0.217\,522 \times 10^{-40}$
32.00	$0.452\,166 \times 10^{-41}$	$0.386\,550 \times 10^{-41}$	60.00	$0.310\,538 \times 10^{-40}$	$0.227\,187 \times 10^{-40}$
33.00	$0.498\,929 \times 10^{-41}$	$0.424\,272 \times 10^{-41}$			

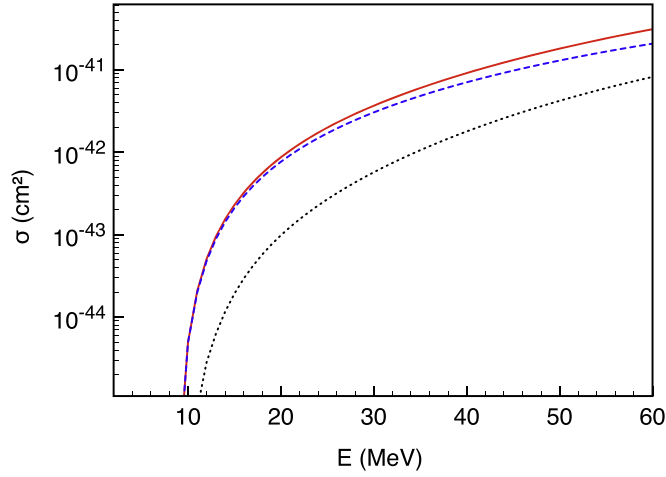


Figure 5. Neutron emission cross sections for neutral-current neutrino scattering on ^{13}C . The total neutron emission cross section, $\nu + ^{13}\text{C} \rightarrow \nu + n + \text{all final states}$ (solid line), cross section for transition to the 0^+ ground state in ^{12}C , $\nu + ^{13}\text{C} \rightarrow \nu + n + ^{12}\text{C}(\text{g.s.})$ (dashed line), and the cross section for transition to the 2^+ state in ^{12}C at 4.44 MeV followed by decay into the ^{12}C ground state, $\nu + ^{13}\text{C} \rightarrow \nu + n + ^{12}\text{C}(2^+) \rightarrow \nu + n + ^{12}\text{C}(\text{g.s.}) + \gamma(4.44 \text{ MeV})$ (dotted line) are shown.

$$\nu + ^{13}\text{C} \rightarrow \nu + n + ^{12}\text{C}(2^+) \leftrightarrow ^{12}\text{C}(\text{g.s.}) + \gamma(4.44 \text{ MeV}). \quad (4.10)$$

Short-baseline reactor neutrino experiments identified a shape distortion in the 5–7 MeV range in the measured neutrino spectrum [35]. This shape distortion appears as an excess over the predicted spectra. A recent proposal suggests [36] a beyond the Standard Model solution to resolve this issue: non-standard neutrino interactions which induce the reaction $^{13}\text{C}(\bar{\nu}, \bar{\nu}' n)^{12}\text{C}^*$ followed by the de-excitation of $^{12}\text{C}^*$ yielding a prompt 4.44 MeV photon. The neutron produced would then lose its kinetic energy scattering off protons yielding scintillation light. It was proposed that this scintillation light along with the prompt photon would mimic the spectral distortion around 5 MeV. To help assess further investigation of such processes we tabulate the Standard Model $^{13}\text{C}(\bar{\nu}, \bar{\nu}' n)^{12}\text{C}^*$ neutrino cross sections in table 5.

Finally a comparison of the various neutron emission cross sections for ν_e interacting with carbon isotopes is given in figure 6. The cross sections are roughly proportional to the phase space of the final states, $(E_\nu - E_{\text{th}})^2$, where E_ν is the initial neutrino energy and E_{th} is the threshold energy for neutron emissions measured from the ground state of the parent nucleus. For neutral-current reactions, E_{th} is equal to the neutron separation energy (S_n), and $E_{\text{th}} = 4.946 \text{ MeV}$ and 18.721 MeV for ^{13}C and ^{12}C , respectively. For charged-current reactions, E_{th} is the sum of S_n in the daughter nucleus and the β^+ -decay Q -value. They are $E_{\text{th}} = 22.284 \text{ MeV}$ ($S_n = 20.064 \text{ MeV}$, $Q = 2.220 \text{ MeV}$) and 32.378 MeV ($S_n = 15.040 \text{ MeV}$, $Q = 17.338 \text{ MeV}$) for ^{13}C and ^{12}C , respectively. The difference in the magnitude of the calculated cross sections in figure 6 can be understood in terms of the difference in the threshold energies except for some details due to the difference between ^{12}C and ^{13}C . In case of neutral-current reaction on ^{13}C , the Gamow–Teller transition to the $1/2^-$ state at $E_x = 8.860 \text{ MeV}$ gives the dominant contribution to the cross section near threshold, that is, at $E_\nu = 9\text{--}12 \text{ MeV}$. At $E_\nu \geq 15 \text{ MeV}$, the Gamow–Teller transition to the $3/2^-$ state at $E_x = 9.898 \text{ MeV}$ gives a contribution comparable to the $1/2^-$ state. In case of neutral-current reaction on ^{12}C , excitations of spin-dipole states (0^- , 1^- and 2^- states) above the threshold energy give more important contributions to the neutron emission cross

Table 5. $^{13}\text{C}(\nu, \nu' n)^{12}\text{C}^*$ and $^{13}\text{C}(\bar{\nu}, \bar{\nu}' n)^{12}\text{C}^*$ neutrino cross sections leading to the 4.44 MeV state in ^{12}C calculated using only the Standard Model interactions.

E (MeV)	$\sigma(\nu)$ (cm ²)	$\sigma(\bar{\nu})$ (cm ²)	E (MeV)	$\sigma(\nu)$ (cm ²)	$\sigma(\bar{\nu})$ (cm ²)
8.00	$5.530\,38 \times 10^{-57}$	0	18.00	$5.768\,96 \times 10^{-44}$	$5.410\,18 \times 10^{-44}$
9.00	$1.152\,14 \times 10^{-53}$	$1.037\,56 \times 10^{-53}$	19.00	$7.641\,58 \times 10^{-44}$	$7.138\,18 \times 10^{-44}$
10.00	$6.120\,58 \times 10^{-48}$	$5.954\,85 \times 10^{-48}$	20.00	9.84805×10^{-44}	$9.162\,68 \times 10^{-44}$
11.00	$7.688\,61 \times 10^{-46}$	$7.429\,09 \times 10^{-46}$	21.00	$1.241\,47 \times 10^{-43}$	$1.150\,38 \times 10^{-43}$
12.00	$2.819\,23 \times 10^{-45}$	$2.708\,49 \times 10^{-45}$	22.00	$1.537\,09 \times 10^{-43}$	$1.418\,34 \times 10^{-43}$
13.00	$6.266\,49 \times 10^{-45}$	$5.985\,53 \times 10^{-45}$	23.00	$1.874\,81 \times 10^{-43}$	$1.722\,47 \times 10^{-43}$
14.00	$1.165\,58 \times 10^{-44}$	$1.109\,49 \times 10^{-44}$	24.00	$2.258\,00 \times 10^{-43}$	$2.065\,20 \times 10^{-43}$
15.00	$1.928\,11 \times 10^{-44}$	$1.829\,82 \times 10^{-44}$	25.00	$2.690\,19 \times 10^{-43}$	$2.449\,04 \times 10^{-43}$
16.00	$2.934\,57 \times 10^{-44}$	$2.774\,18 \times 10^{-44}$	26.00	$3.175\,05 \times 10^{-43}$	$2.876\,53 \times 10^{-43}$
17.00	$4.206\,74 \times 10^{-44}$	$3.960\,67 \times 10^{-44}$	27.00	$3.716\,42 \times 10^{-43}$	$3.350\,24 \times 10^{-43}$

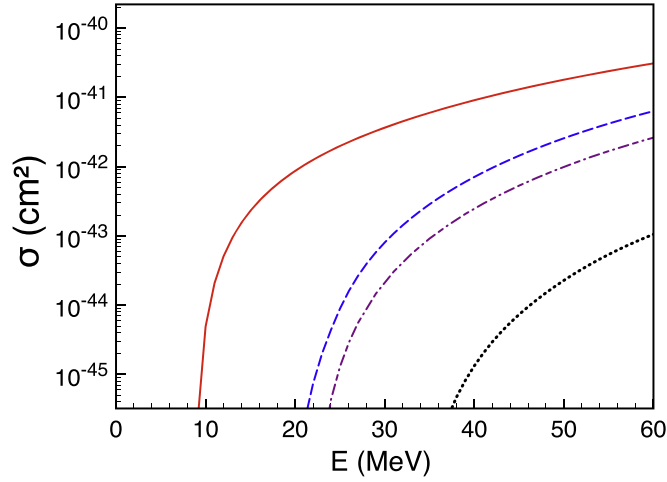


Figure 6. A comparison of the neutron emission cross sections for ν_e interacting with carbon isotopes. Neutral-current contribution to neutron emission in the reaction $\nu + {}^{13}\text{C}$ (solid line), neutral-current contribution to neutron emission in the reaction $\nu_e + {}^{12}\text{C}$ (dashed line), charged-current contribution to neutron emission in the reaction $\nu + {}^{13}\text{C}$ (dotted-dashed line), and charged-current contribution to neutron emission in the reaction $\nu_e + {}^{12}\text{C}$ (dotted line). The ${}^{12}\text{C}$ data is taken from [33].

section than those of 1^+ states. Note that the 1^+ state at $E_x = 15.11$ MeV with the largest magnetic dipole strength is below the neutron emission threshold.

5. Conclusions

Since ${}^{13}\text{C}$ is naturally present in carbon-based scintillators, it is important to know its interaction cross section with neutrinos to achieve high precision in neutrino experiments using such scintillators. In an earlier publication we presented calculations of those cross sections at reactor neutrino energies. In this paper these cross sections both for charged-current and neutral-current reactions are given at higher energies, relevant to terrestrial supernova observations and measurements at the spallation neutron sources (such as the Oak Ridge facility used in the experiment of [32]). Since there are ongoing and planned neutrino coherent scattering experiments at those spallation neutron sources, those cross sections are also provided. Since the processes with neutrons are present in the final state and could provide a convenient signal via the 2.2 MeV photons as well as help in the searches for physics beyond the Standard Model we provided the Standard Model values of the cross section for those processes as well.

Acknowledgments

This work was supported in part by Grants-in-Aid for Scientific Research of JSPS (15H03665, 15K05090, 17K05459), in part by the US National Science Foundation Grants No. PHY-1806368 and PHY-1630782. ABB is also supported in part by the visiting professor program at the National Astronomical Observatory of Japan.

ORCID iDs

A B Balantekin  <https://orcid.org/0000-0002-2999-0111>

References

- [1] Suzuki T, Fujimoto R and Otsuka T 2003 *Phys. Rev. C* **67** 044302
- [2] Adey D *et al* (Daya Bay Collaboration) 2018 *Phys. Rev. Lett.* **121** 241805
- [3] Bak G *et al* (RENO Collaboration) 2018 *Phys. Rev. Lett.* **121** 201801
- [4] Kaneda M and Double Chooz Collaboration 2018 *Phys. Part. Nuclei* **49** 709
- [5] Agostini M *et al* (BOREXINO Collaboration) 2018 *Nature* **562** 505
- [6] Miramonti L and JUNO Collaboration 2018 *Universe* **4** 126
- [7] Wurm M *et al* (LENA Collaboration) 2012 *Astropart. Phys.* **35** 685
- [8] Athanassopoulos C *et al* (LSND Collaboration) 1997 *Phys. Rev. C* **55** 2078
- [9] Arafune J, Fukugita M, Kohyama Y and Kubodera K 1989 *Phys. Lett. B* **217** 186
- [10] Fukugita M, Kohyama Y, Kubodera K and Kuramoto T 1990 *Phys. Rev. C* **41** 1359
- [11] Cohen S and Kurath D 1965 *Nucl. Phys.* **73** 1
- [12] Millener D J and Kurath D 1975 *Nucl. Phys. A* **255** 315
- [13] Arima A, Shimizu K, Bentz W and Hyuga H 1987 *Adv. Nucl. Phys.* **18** 1
- [14] Pourkaviani M and Mintz S L 1991 *J. Phys. G: Nucl. Part. Phys.* **17** 1139
- [15] Mintz S L 2000 *Nucl. Phys. A* **672** 503
- [16] Suzuki T, Balantekin A B and Kajino T 2012 *Phys. Rev. C* **86** 015502
- [17] Scholberg K 2012 *Annu. Rev. Nucl. Part. Sci.* **62** 81
- [18] Dasgupta B and Beacom J F 2011 *Phys. Rev. D* **83** 113006
- [19] Kuo T T S 1967 *Nucl. Phys. A* **103** 71
- [20] Suzuki T, Chiba S, Yoshida T, Kajino T and Otsuka T 2006 *Phys. Rev. C* **74** 034307
- [21] Otsuka T, Suzuki T, Fujimoto R, Grawe H and Akaishi Y 2005 *Phys. Rev. Lett.* **95** 232502
- [22] Suzuki T and Kajino T 2013 *J. Phys. G: Nucl. Part. Phys.* **40** 083101
- [23] Walecka J D 1975 *Muon Physics* ed V H Hughes and C S Wu vol 2 (New York: Academic)
- [23] O'Connell J S, Donnelly T W and Walecka J D 1972 *Phys. Rev. C* **6** 719
- [23] Donnelly T W and Walecka J D 1976 *Nucl. Phys. A* **274** 368
- [23] Donnelly T W and Haxton W C 1979 *At. Data Nucl. Data Tables* **23** 103
- [24] Walter R L and Guss P P 1986 *Proc. Int. Conf. on Nuclear Data for Basic and Applied Science* vol 2 ed P G Young (New York: Gordon and Breach) p 1079
- [25] Avrigeanu V, Hodgson P E and Avrigeanu M 1994 *Phys. Rev. C* **49** 2136
- [26] Belgia T *et al* 2006 *Handbook for Calculations of Nuclear Reaction Data: Reference Input Parameter Library* (Vienna: IAEA) <http://nds.iaea.org/RIPL-2/>
- [27] Ianni A, Montanino D and Villante F L 2005 *Phys. Lett. B* **627** 38
- [28] Bolozdynya A *et al* arXiv:1211.5199 [hep-ex]
- [29] Freedman D Z 1974 *Phys. Rev. D* **9** 1389
- [30] Freedman D Z, Schramm D N and Tubbs D L 1977 *Annu. Rev. Nucl. Part. Sci.* **27** 167
- [31] Drukier A and Stodolsky L 1984 *Phys. Rev. D* **30** 2295
- [32] Akimov D *et al* (COHERENT Collaboration) 2017 *Science* **357** 1123
- [33] Yoshida T, Suzuki T, Chiba S, Kajino T, Yokomakura H, Kimura K, Takamura A and Hartmann D H 2008 *Astrophys. J.* **686** 448
- [34] Patton K, Engel J, McLaughlin G C and Schunck N 2012 *Phys. Rev. C* **86** 024612
- [35] Balantekin A B 2016 *Eur. Phys. J. A* **52** 341
- [36] Berryman J M, Brdar V and Huber P 2019 *Phys. Rev. D* **99** 055045